Journal of
Materials Chemistry C

Accepted Manuscript

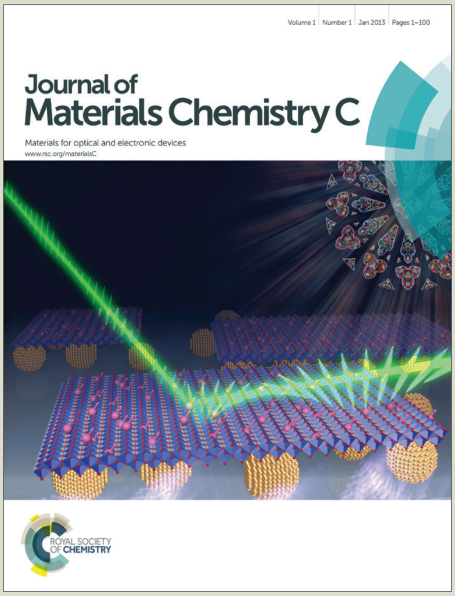

Volume 1 | Number 1 | Jan 2013 | Pages 1–100

Journal of
Materials Chemistry C

Materials for optical and electronic devices
www.rsc.org/materialsC

ROYAL SOCIETY
OF CHEMISTRY

ROYAL SOCIETY
OF CHEMISTRY

www.rsc.org/materialsC

High carrier mobility of few-layer PbX (X = S, Se, Te)

Xi-Bo Li[1], Pan Guo[1,2], Yan-Ning Zhang [1,3], Ru-Fang Peng[2], Hui Zhang[1], Li-Min Liu[1]*

[1]Beijing Computational Science Research Center, Zhongguancun Software Park Ⅱ,
Dongbeiwang West Road, Haidian District, Beijing 100094, China
[2]State Key Laboratory Cultivation Base for Nonmetal Composites and Functional Materials, Southwest University of Science and Technology, Mianyang, Sichuan, 621010, China
[3] Chengdu Green Energy and Green Manufacturing Technology R&D Center,
Chengdu, Sichuan, 610207, China
Email: limin.liu@csrc.ac.cn
Tel: +86-10-5698 1827

Two-dimensional materials with higher carrier mobility are promising materials for applications in the nanoelectronics and photocatalysis. In this paper, we have explored the stabilities, structures, electronic properties, carrier mobility and optical properties of few-layer PbX (X = S, Se, Te) by first-principle calculations. Theoretical results show that the band gaps of PbX could be modulated by the thickness, changing from 1.65 eV (1.26 eV, 1.26 eV) of monolayer to 0.98 eV (0.76 eV, 0.97 eV) of tri-layer for PbS (PbSe, PbTe). Most importantly, the bi-layer PbS has an extremely high electron carrier mobility of 252 000 $cm^2V^{-1}s^{-1}$ and the hole carrier mobility of mono- or tri-layer PbTe could obtains a value of 16 000 $cm^2V^{-1}s^{-1}$, predicating the possible wide applications of few-layer PbXs in novel electronic devices. The strong adsorptions of light of PbXs also indicate their potential implications in solar cell.

1. Introduction

Two-dimensional (2D) materials have excited intensive studies for decades because of their novel electronic and optical properties. Typical 2D material, such as graphene or carbon based 2D materials[1-9], boron nitride (BN)[10], transition metal dichalcogenides (TMDs)[11-14], and black phosphorus (BP)[15-19], are investigated for applications in high-performance electronic devices in field-effect transistors (FETs)[5, 14, 18], thin-film solar cell[20, 21], thermoelectric devices[22, 23] and lithium-ion batteries[17, 24]. As a candidate 2D material used in FETs, there are three basic requirements: a moderate electronic band gap, high carrier mobility and excellent electrode-channel contacts[4, 12, 20, 25, 26]. Therefore, the 2D materials with semiconductive characteristic have attracted lots of researches for their potential applications in FETs. For example, the carrier mobility in ultra-thin $MoSe_2$ layers could be 50 $cm^2V^{-1}S^{-1}$ at room temperature[14], and that in the monolayer MoS_2[12] could even reach to a high value of 200 $cm^2V^{-1}S^{-1}$. Recently, researches show that the carrier ability of monolayer black phosphorus (M-BP) is as high as 286 $cm^2V^{-1}S^{-1}$ in experiment[17] and even higher in theoretical calculations[18], a promising candidate in FETs. However, the stability of black phosphorus at room and high temperatures will be one problem as the combustible matter. Thus, it is fascinating to explore suitable 2D materials, which have direct and proper band gap, as well as high carrier mobility for application in FETs. The new 2D materials can be predicted based on bulk materials or by advanced particle swarm optimization algorithm (PSO)[27].

The bulk lead chalcogenides[28, 29] PbX, (X = S, Se, Te) have the cubic NaCl structure (space group Fm3m) and the direct narrow-gaps make them important in FETs[28, 30], thermoelectric devices[31-33] and solar-energy panels[34]. In this work, the atomic structures and physical properties of few-layer PbXs are explored theoretically in the frame of density function theory (DFT). Stabilities of the few-layers are verified by the phonon bands and formation energies. Then, the band gap, carrier mobility and optical properties of few-layer PbXs are discussed. The tunable band gap and high carrier mobility indicate the high performance of few-layer PbX (X = S, Se, Te) in applications in nanoelectronics and optoelectronics. The calculated adsorption of light indicates the potential applications of few-layer PbXs in solar cell.

2 Method

The calculations were carried out with DFT implemented in the Vienna ab-initio simulation package (VASP)[35]. The exchange–correlation potential was described by the generalized gradient approximation (GGA) functional of Perdew, Burke, and Ernzerhof (PBE)[36]. The van der Waals (vdW) correction proposed by Grimme[37] (DFT-D3) was included in our calculations expect the bulk case to obtain the correct structures. The plane wave cut-off energy was chosen to be 500 eV. A 8×8×1 k-point sampling based on Gama-centered Monkhorst-Pack scheme[38] was used for all the structural relaxation. The structural optimization process for all atoms was finished until the final force on each atom was less than 2×10^{-3} eV/Å and the total energy change was less than 10^{-6} eV. Meanwhile, a vacuum space of 15 Å was added in the unit cell to avoid the interaction between the repeated unit cells.

The stability of 2D material can be determined from the formation energy, which is defined as follows:

$$E_f = E_{2D}/N_{2D} - E_{3D}/N_{3D} \qquad (1)$$

where E_{2D} and E_{3D} represent the energies of few-layer and bulk PbX, respectively; N_{2D} and N_{3D} denote the number of atoms in primitive cell of few-layer and bulk PbX in our calculations. The smaller formation energy the 2D material has, the more stable it becomes.

The carrier mobility in 2D material can be estimated by the phonon-limited formula[39, 40]:

$$\mu = (e\hbar^3 C_{2D})/[k_B T m_e^* m_d (E_i)^2] \qquad (2)$$

where m_e^* is the effective mass along the transport direction (either m_x or m_y along the x or y direction, respectively), and m_d is the equivalent density-of-state mass defined as $m_d = \sqrt{(m_x m_y)}$.The deformation potential $E_i = \triangle E_i/(\triangle L_i/L_i)$ is computed through the energy change induced by the lattice compression or dilatation of few-layer PbX by a step of $\triangle L_i/L_i = 0.005$ in the transport direct. What should be noted is that, the E_i of valance band minimum (VBM, E_h) is for hole and that of conduction band maximum (CBM, E_e) is for electron. The elastic moduli of the longitudinal acoustic C_{2D} in the propagation direction is defined as $C_{2D} = 2(E - E_0)/[S_0\,(\triangle L_i/L_i)^2]$, where E and E_0 are the total energy with lattice changes in i direction and at equilibrium state, respectively, and the S_0 is the area of the 2D material at equilibrium state.

Optical property is obtained by calculating the frequency dependent dielectric matrix. The imaginary part is determined by a summation over empty states using the equation[41]:

$$\varepsilon^2_{\alpha\beta}(\omega) = \frac{4\pi^2 e^2}{\Omega} \lim_{q\to 0} \frac{1}{q^2} \sum_{c,v,\mathbf{k}} 2\omega_{\mathbf{k}} \delta\left(\varepsilon_{c\mathbf{k}} - \varepsilon_{v\mathbf{k}} - \omega\right) \times \left\langle u_{c\mathbf{k}+\mathbf{e}_\alpha q} \mid u_{vk} \right\rangle \left\langle u_{c\mathbf{k}+q\mathbf{e}_\beta} \mid u_{v\mathbf{k}} \right\rangle^* \qquad (3)$$

where the indices Ω, ω, c, v refer to the unit-cell volume, photon frequencies, conduction and valence band states, respectively, $u_{c\mathbf{k}}$ is the cell periodic part of the orbitals at the k-point $\mathbf{k}$. The vectors $\mathbf{e}_\alpha$ are unit vectors for the three Cartesian directions.

3 Results and Discussions

3.1 Stability of monolayer PbX (X = S, Se, Te)

The calculated lattice parameters of bulk PbS, PbSe, and PbTe are $a_{bulk} = b_{bulk} = c_{bulk}$ = 5.922 Å, 6.125 Å, 6.464 Å, respectively, all within the error of 0.3% experiment[29] (see **Table 2**), indicating the accuracy of our PBE method. These values are then used to determine the planer lattice parameters of few-layer PbX. The initial configurations of the few-layer PbXs are cleaved along the [001] direction from the bulk PbXs. Each monolayer contains two sublayers, and the few-layer PbXs are consisted with several corresponding monolayers. The monolayer PbX, which includes 2 Pb atoms and 2 X atoms in an unit cell, contains two sublayers along [001] direction of bulk PbX with X (Pb) atom on Pb (X) atom, as shown in **Fig. 1. (b)**. The vector relationship between the monolayer bulk and the are: $\mathbf{a}=1/2(a_{\mathrm{bulk}}\mathbf{e}_x+b_{\mathrm{bulk}}\mathbf{e}_y)$, $\mathbf{b}=1/2(a_{\mathrm{bulk}}\mathbf{e}_x-b_{\mathrm{bulk}}\mathbf{e}_y)$, here $\mathbf{e}_x$ ($\mathbf{e}_y$) is the lattice direction in bulk *xy* plane.

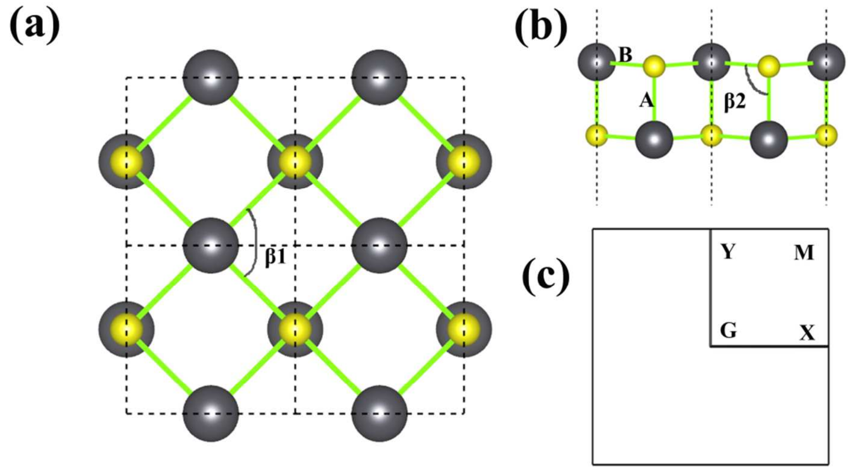

Fig. 1 Top (a) and side (b) views of atomic structures of monolayer and bi-layer PbX (X=S, Se, and Te) and associated first Brillioiun zone (c). The lattice parameter *a* is equal to *b* in *xy* plane and the structural parameters are labeled as (**A**, **B**, β1, β2). The **A** and **B** refer to the bond between X atom and nearest Pb atom in different sublayers and in the same sublayer, respectively. β1 (β2) indicates the angle of X-Pb-X (Pb-X-Pb) with X (Pb) atoms nearest to Pb (X) atom in the same sublayer (different sublayers).

To provide a rigorous proof for the stability of monolayer PbXs, the phonon band structures of optimized structures were calculated by force constant approach[42] implanted in Phonopy package. The phonon frequencies of monolayer PbX were obtained as following. First, a set of 4×4×1 supercells with atoms displacements was generated according to relaxed unit cell and symmetry restriction of monolayer PbX. Second, the forces on the atoms of each supercell were calculated by VASP with a 3×3×1 k-point sampling based on Gama-centered Monkhorst-Pack scheme. Then the corresponding forces were collected and used for phonon frequencies calculations of PbX by Phonopy. The structure is stable only when the frequencies of all phonon bands are positive. The phonon band structures of the monolayer PbXs in **Fig. 2** show positive frequencies, except very tiny imaginary frequencies near the Γ points ($k\rightarrow0$) for PbS and PbSe. Accordingly, we could conclude that the monolayer PbX (X=S, Se, Te) is thermodynamically stable.

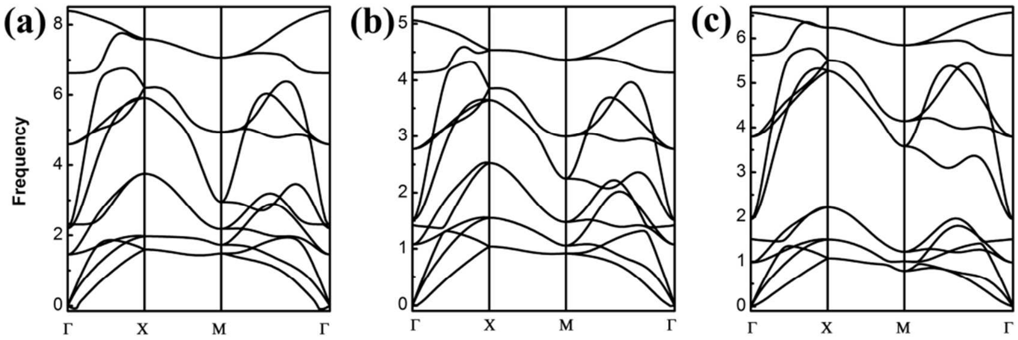

Fig. 2 Phonon band structure of (a) PbS, (b) PbSe, and (c) PbTe monolayers with 4×4×1 supercell, respectively.

The formation energies, E_f, calculated according to **Eq. 1**, decrease as the number of PbX layer grows from one to three: E_f changes from 0.18 eV to 0.07 eV for PbS, from 0.20 eV to 0.08 eV for PbSe, from 0.21 eV to 0.08 eV for PbSe, as listed in **Table 1**. We have shown the stability of the monolayer PbXs through the phonon band structures in the paragraph above, so we may expect more stable few-layer PbXs.

Table 1 Formation energies of PbX (X=S, Se, Te) for monolayer to tri-layer.

Type/Layer	1L	2L	3L
PbS (eV)	0.18	0.10	0.07
PbSe (eV)	0.20	0.12	0.08
PbTe (eV)	0.21	0.12	0.08

3.2 Atomic structures and electronic properties of few-layer PbX

Once the stabilities of the few-layer PbX were confirmed, atomic structures, electronic and optical properties are explored in the following. As shown in **Table 2**, the lattice parameters of PbS, PbSe, PbTe increase by 0.007 Å, 0.031 Å, 0.079 Å (a_{2D}-$a_{bulk}/\sqrt{2}$), comparing with the corresponding values in bulk, respectively. Meanwhile, the Pb and X atoms in the same sublayer in bulk structures become bulkling in the 2D PbX: the Se and Te atoms are 0.034 Å and 0.302 Å higher than the coplanar Pb atom along the normal direction in PbSe and PbTe, respectively, whereas S atom is 0.156 Å lower than Pb atom in PbS. The bond lengths of Pb-S, Pb-Se, or Pb-Te along the normal direction, denoted as type **A**, are 2.693 Å, 2.825 Å, or 3.033 Å, respectively, which are 0.277 Å, 0.260 Å, 0.288 Å shorter than the corresponding bonds in the same sublayer, denoted as type **B**. The bulkling character and the different bond lengths result from the appearance of dangling bonds in the few-layers, which makes the interaction between Pb and X atom in the *z* direction strong. For bi-layer PbXs, the bond lengths of Pb-S, Pb-Se, or Pb-Te, denoted as type A (B) are 2.769 Å (2.962 Å), 2.886 Å (3.068 Å), or 3.073 Å (3.252 Å), increased (decreased) by 0.076 Å (0.008 Å), 0.061 Å (0.017 Å), 0.040 Å (0.069 Å) while comparing with corresponding ones of monolayer, respectively. The distance of the two monolayers is

3.192 Å, 3.224 Å, 3.374 Å for PbS, PbSe, and PbTe, respectively, which is about 0.423 Å, 0.338 Å, 0.301 Å longer than length of bond type **A**, about 0.230 Å, 0.156 Å, 0.122 Å larger than that of bond type **B**. Those parameters indicate the interaction between layers is somewhat of chemical rather than vdW interaction, which leads to the interlayer interaction of two-layer PbS, PbSe, and PbTe with a value of 0.64 eV, 0.68 eV, and 0.72 eV, respectively (see **Table 1**). In additional, we take bi-layer PbS as an example to check the effect of vdW correction. Comparing the calculations with and without vdW correction, the distance between two monolayers of bilayer PbS is 3.303 Å without considering vdW correction, which is about 0.111 Å larger than the one with vdW correction.

Table 2 The theoretical lattice constants and the calculated band gap of few layer and bulk PbX(X=S, Se, Te) compared with to previous experiment results.

	PbS			**PbSe**			**PbTe**		
	a_0/Å	β1/β2°	**Gap/eV**	**a_0**	β1/β2°	**Gap**	**a_0**	β1/β2°	**Gap**
1	4.194	89.84/93.01	1.65	4.362	90.00/89.37	1.26	4.650	89.52/84.75	1.26
2	4.188	89.97/91.32	1.23	4.338	89.97/88.71	0.94	4.583	89.62/85.30	1.07
3	4.185	89.97/91.32	0.98	4.332	89.97/88.71	0.76	4.576	89.71/85.95	0.97
Bulk	5.922	89.99/90.79	0.34	6.125	90.00/90.00	0.30	6.464	90.00/90.00	0.74
Exp[29]	5.936		0.41	6.124		0.28	6.462		0.31

The calculated band structures of bulk PbS, PbSe and PbTe are similar, owning a direct band gap at L point with a value of 0.34 eV, 0.30 and 0.74 eV (see **Fig. 3(a), Fig. 4(a), Fig. 4(c)**). The corresponding experimental results are 0.41 eV, 0.28 eV, and 0.31 eV[29], respectively. Clearly, the band gaps of bulk PbS and PbSe could be well predicted by PBE calculations, but that of PbTe are overestimated in our results as spin-orbit coupling effect is not include in our calculations[43]. The The hole (VBM) and electron (CBM) effective mass at L point for bulk PbS, PbSe, PbTe are 0.119 m_0 and 0.145 m_0, 0.120 m_0 and 0.106 m_0, 0.121 m_0 and 0.097 m_0, respectively. These results are in the range of experiments[29, 44] and previous theory calculations[43]. The effective masses of PbXs obtained from PBE method are nearly the same as that of experiments result[29, 44] (within range 0.07~0.20 m_0), which indicating the PBE could predict the effective mass with a reliable accuracy. Thus, although the band gap of PbTe calculated with PBE is obviously larger than the experimental one without considering the spin-orbital coupling[44], the calculated effective mass with PBE is very close to the experimental ones.

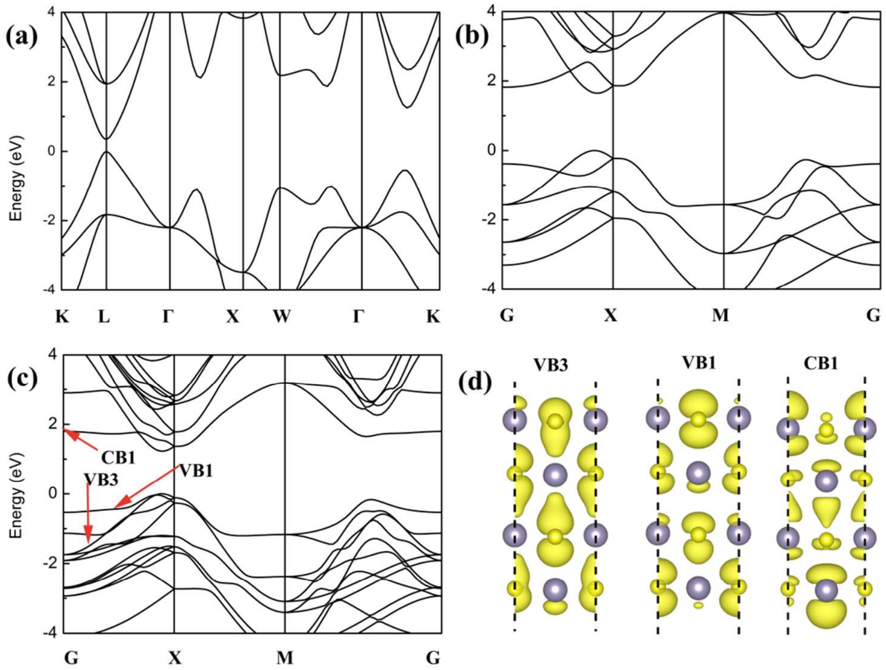

Fig. 3 Band structures of (a) bulk and (b) monolayer (c) bi-layer PbS. (d) Charge distribution of correspond states of bi-layer PbS labeled in (c). The isovalue is set to 0.003 e/bohr^3. The Fermi level is set to zero.

Then we focus on the electronic properties of few-layer PbXs. In monolayer, the Γ point in the bulk BZ folds backs to the G point, so the G-L and X-W directions in the bulk BZ will be projected to the G-X and G-M directions of monolayer ones. As shown in Figs. 3(b), 4(b), and 4(d), the monolayer PbXs own direct band gaps along the G-X directions at the (0.425, 0, 0) point. The band gaps of the monolayer PbS, PbSe, and PbTe are 1.65 eV, 1.26 eV and 1.26 eV, respectively. It's interesting that the band gap of a bi-layer PbX is reduced to 1.23 eV, 0.94 eV and 1.07 eV for PbS, PbSe, and PbTe, respectively. To further understand the reduction of the band gap, we take bi-layer PbS as an example and calculate the charge distribution of correspond states. As shown in Fig. 3, the highest valance band, VB1, and the lowest conduction band, CB1, bond two layers, whereas the third highest valance band, VB3, indicates the bonding within the monolayer. The work function of the monolayer and bi-layer PbS are nearly the same. This indicates that the bonding between two layers shifts CB1 to lower energy, leading to the reduction of the band gap. Thus, when coupling two monolayers into a bi-layer, the chemical bonding rather than vdW interaction dominates the interaction between two monolayers, which increases the interlayer binding energy and reduces the band gap. When the few-layer PbX becomes thicker, the interaction between layers will be stronger, leading to a smaller band gap and more stable system. These predications are verified by the DFT calculations of the tri-layer cases, as the band gaps of tri-layer PbS, PbSe and PbTe are 0.98 eV, 0.76 and 0.74 eV (See **Table 2**) and the formation energies of tri-layers become smaller (**See Table 1**).

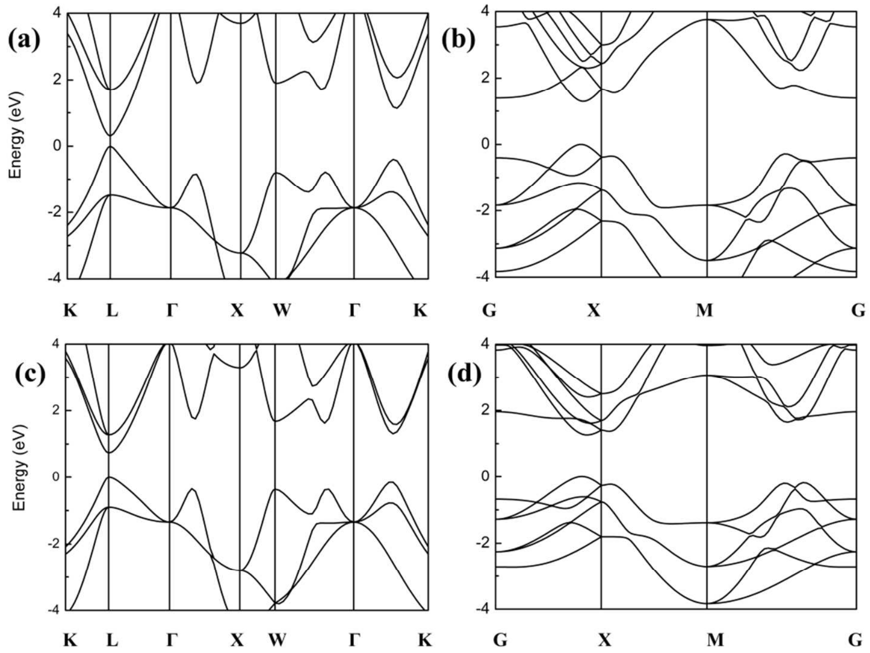

Fig. 4 Band structures of (a) bulk and (b) monolayer PbSe, the corresponding ones of PbTe are listed as (c) and (d), respectively. The Fermi level is set to zero.

3.3 Carrier mobility of Few-layer PbX

The effective masses of monolayer PbX exhibit different behaviors for electron (m_e^*) and hole (m_h^*): m_e^* of PbS, PbSe, PbTe along G-X are 0.170 m_0, 0.126 m_0, 0.169 m_0, only larger than the corresponding bulk values by 0.025 m_0, 0.006 m_0, 0.048 m_0, respectively. On the other hand, the m_h^* of those at VBM along G-X are 0.221 m_0, 0.156 m_0, 0.190 m_0, greatly increased by 0.102 m_0, 0.050 m_0, 0.058 m_0. These values are much smaller than that of MoS_2[45] with 0.48 m_e, h-BN[40] with 0.99 m_e. The m_e^* of few-layer PbS along G-X shows a negative layer-dependence character, as shown in **Table 3**: it decreases from 0.170 m_0 of the monolayer to 0.153 m_0 of tri-layer, which is very close to 0.145 m_0 of bulk one.

The small effective masses of few-layer PbXs indicate the possible inherence of high carrier mobility from the bulk ones. The carrier mobility for 2D systems is calculated by applying the **Eq. 2**. Due to the symmetry of *x*- and *y*-axes, the properties along the two directions are same, thus we focus on one direction. The predicted carrier mobilities of few-layer PbXs are very large, as list in **Table 3**, and the electron mobility is much larger than hole for PbS and PbSe. The electron carrier mobility for monolayer PbS will reach a moderate value of 72 850 $cm^2V^{-1}s^{-1}$, more than 30 times of than the hole. The difference mainly results from the small deformation potential E_e for electron at CBM, compared with that of deformation potential E_h for hole at VBM (See **Table 3**). In the bi-layer PbS, the electron carrier mobility becomes extraordinarily large, with a value of about 252 610 $cm^2V^{-1}s^{-1}$. The even smaller E_e, m_e^* and larger C_{2D} are the main reasons. The electron (hole) mobility of tri-layer PbS moves to relative smaller values because of the larger deformation potential. Similar trend happens to few-layer PbSe, with a maximum value of electron mobility of 74 630 $cm^2V^{-1}s^{-1}$ for bi-layer. However, the hole carrier mobility of monolayer PbTe is nearly two times as that of electron, with a value of 16 580 $cm^2V^{-1}s^{-1}$. The large carrier mobilities indicate that the monolayer and bi-layer PbS or PbSe may have high performance in transport of electron in FETs.

According to **Eq. 2**, the factors that lead to the extremely high carrier mobility of PbX include both a small effective mass and a large elastic moduli. The elastic moduli of PbS, PbSe and PbTe are nearly 57 J/m^{-2}, 48 J/m^{-2}, and 33 J/m^{-2} per layer, which is larger than that of few-layer phosphorus[18] of 30 J/m^{-2}. The decrease of C_{2D} shows that the interaction of Pb and X atoms becomes weak while changing X atom from S atom to Te atom. More importantly, the deformation potentials of few-layer PbXs are extremely small. The deformation potential E_e for electron of mono-, bi-layer PbS and PbSe could reach values of 0.71 eV, 0.60 eV, 1.27 eV, 1.19 eV, respectively, much smaller than other materials applied in FETs, mainly in range of 3.7~5.0 eV[40, 45-47]. In details, while comparing monolayer MoS_2 with monolayer PbS, the deformation potential $\boldsymbol{E_e}$ (the effective electron mass at CBM) for MoS_2 is 5.50 (2.82) [47] times of that for monolayer PbS, and the corresponding carrier mobility of PbS is about 89.32 times larger than that of MoS_2 if only considering these two factors. Thus, the low deformation potential and effective mass are critical to the high mobility of PbXs. The small E_e is in essence related to the bonding character of CBM. There are nearly no bonding characteristics for Pb atom and S atom in the *xy* plane for CBM and VBM, causing a small change of charge distribution of the CBM and VBM of few-layer PbX [see bi-layer case in **Fig. 3(d)**]. So the structural deformation introduced along *x* (or *y*) direction have little effect on the nonbonding character (or isolated charge distribution) of CBM in *xy* plane, and leads to a very small E_e. Similarly, the un-bonded character of VBM will also lead to a small E_h, but still larger than that of electron (except the few-layer PbTe). The different deformational potentials of E_e and E_h could also be explained by the different bonding characteristics of VBM and CBM. For example, as for bi-layer PbS, the CBM has overlapping along z direction while the VBM does not have such feature [**See Fig. 3(d)**], whereas the bond between Pb and S atom in the *z* direction is nearly unaffected through deformation, and also the deformation is even less for electron (CBM) than for hole (VBM) as less electron distribution in *xy* plane, thus the deformational potential for E_e is even smaller than E_h. And also, the values E_h for hole and E_e for electron of mono- or bi-layer PbS and PbSe are nearly layer independent. We note that the E_h and E_e of tri-layer PbS are much larger than those for the mono- and bi-layer ones, as tri-layer one behaviors more like bulk ones. However, the $E_{e(h)}$ for few-layer PbTe show layer-dependent strongly and are more complicated. While forming multilayer PbTe from monolayers, the prior VB and CB of monolayers could couple because of the interaction between layers. Thus, the coupling effect could make few-layer PbTe deformation potential larger (See **Table 3**, except $\boldsymbol{E_h}$ of tri-layer PbTe), make the multilayer PbTe stable (see **Table 1**).Interestingly, the E_h becomes smaller whereas the electron E_e becomes bigger from few-layer PbS to PbTe. Along with the analysis above, more un-delocalized charge distribution of VBM and the weaker bonding character of CBM between different layers of PbX in the *z* direction while X atom changing from S to Te atom lead to the trend of mobility, and the effect of the former becomes lager than the latter, the hole E_h may be smaller than the electron E_e, as see the few-layer PbTe in **Table 3**.

Table 3 Carrier mobility of few layer PbX (X=S, Se, Te) predicted by theoretical calculations at 300K. The $\boldsymbol{m_e^*(m_h^*)}$, $\boldsymbol{E_e(E_h)}$ and $\boldsymbol{\mu_e(\mu_h)}$ indicate the effective mass, deformation potential, carrier mobility for electron at CBM (hole at VBM), C_{2D} is the elastic moduli along *x* direction.

	Layer	$\boldsymbol{m_e^*}$	$\boldsymbol{m_h^*}$	$\boldsymbol{E_e}$	$\boldsymbol{E_h}$	$\boldsymbol{C_{2D}}$	$\boldsymbol{\mu_e}$	$\boldsymbol{\mu_h}$
Units		$\boldsymbol{m_0}$		**eV**		**Jm^{-2}**	**10^{3}cm^{2}V^{-1}s^{-1}**	
PbS	**1**	0.170	0.221	0.710	3.594	56.78	72.85	2.19
	2	0.158	0.199	0.600	3.798	119.63	252.61	5.01
	3	0.153	0.267	3.081	7.086	185.75	13.45	1.45
PbSe	**1**	0.126	0.156	1.273	2.909	48.25	35.92	5.58
	2	0.140	0.146	1.189	3.063	101.30	74.63	11.02
	3	0.146	0.158	2.059	3.028	164.94	37.40	15.96
PbTe	**1**	0.169	0.190	1.705	1.099	32.87	7.95	16.58
	2	0.192	0.172	2.107	2.516	75.08	10.33	8.08
	3	0.547	0.185	3.735	1.690	129.56	1.14	16.42

3.4 Optical adsorption of few-layer PbX

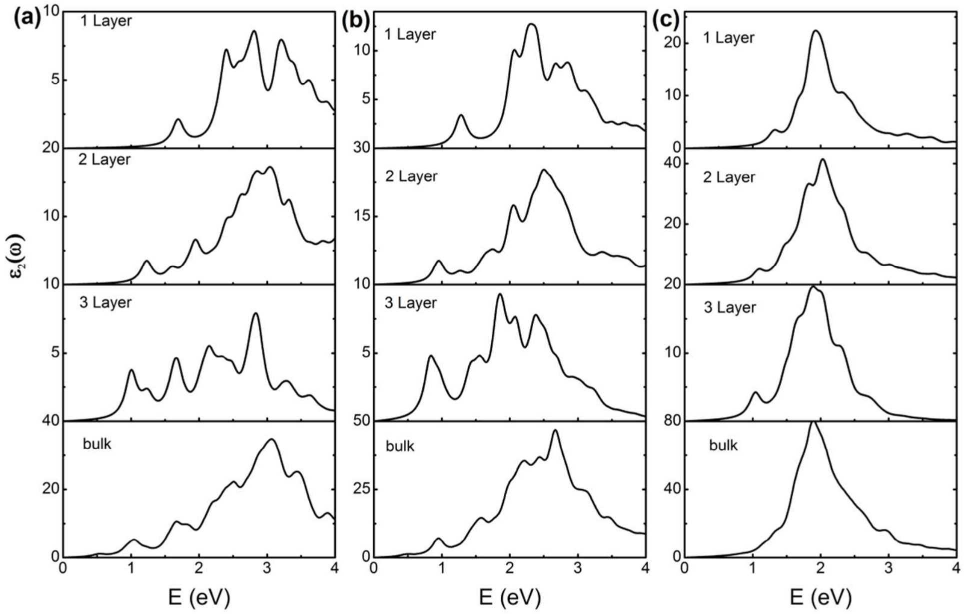

Fig. 5 Calculated imaginary part ε2(ω) of dielectric function of few layer and bulk PbS (a), PbSe (b), PbTe(c) for light incident in *z* direction and polarized along *x* direction.

To explore the optical properties of the few-layer PbX, the dielectric functions are calculated according to the **Eq. 3** and adsorption (also imaginary) part $\varepsilon_2(\omega)$ is depicted in **Fig. 5**. Clearly the first peak of the adsorption spectra strongly relates with band edge that drops with the increase of the thickness, e.g, from 1.65 eV for monolayer to 0.34 eV for bulk PbS. Also, the results show that the adsorption of light among 1.23~3.20 eV is relative larger, indicating the potential implications in solar cell. It should be noted that the spin-orbital coupling effect has great effect on the $\varepsilon_2(\omega)$ of bulk PbSe and PbTe as shown in the previous work[48]. Although the spin-orbital coupling effect is not considered in our calculations, $\varepsilon_2(\omega)$ for bulk PbSe and PbTe exhibit similar features as the previous ones that the maximum $\varepsilon_2(\omega)$ of PbTe is larger than that of PbSe[48] as shown in **Fig. 5**.

4 Conclusions

In summary, we have systemically explored the stabilities, structures, electronic properties, carrier mobility and optical properties of few-layer PbX (X=S, Se and Te). Theoretical calculations show that the band gaps of PbX could be modulated by the thickness, varying from 1.65 eV (1.26 eV, 1.26 eV) of monolayer to 0.98 eV (0.76 eV, 0.97 eV) of tri-layer PbS (PbSe, PbTe). The carrier mobility and optical adsorption are also thickness dependent. Careful studies clearly indicate the few-layer PbS and PbSe own extremely high electron carrier nobilities: >10 000 $cm^2V^{-1}s^{-1}$ for PbS and PbSe few-layers and even higher value of 252 610 $cm^2V^{-1}s^{-1}$ for bi-layer PbS. As a comparison, the few-layer PbTe mainly owns higher hole carrier mobility, such as a value of 16 580 $cm^2V^{-1}s^{-1}$ for monolayer PbTe. The high mobility predicts the wide applications of few-layer PbX (X=S, Se, Te) in modern electronic devices, especially for novel FET devices. In additional, the adsorption of light among indicates the potential implications in solar cell.

Acknowledgments

This work was supported by the National Natural Science Foundation of China (No. 51222212), the MOST of China (973 Project, Grant NO. 2011CB922200). Open Project of State Key Laboratory Cultivation Base for Nonmetal Composites and Functional Materials (11zxfk16).

Reference

1. K. S. Novoselov, A. K. Geim, S. V. Morozov, D. Jiang, Y. Zhang, S. V. Dubonos, I. V. Grigorieva and A. A. Firsov, *Science*, 2004, **306**, 666-669.

2. A. K. Geim and K. S. Novoselov, *Nat.Mater*, 2007, **6**, 183-191.
3. A. A. Balandin, *Nat.Mater*, 2011, **10**, 569-581.
4. L. Liao, Y.-C. Lin, M. Bao, R. Cheng, J. Bai, Y. Liu, Y. Qu, K. L. Wang, Y. Huang and X. Duan, *Nature*, 2010, **467**, 305-308.
5. F. Schwierz, *Nat Nano*, 2010, **5**, 487-496.
6. A. Du, S. Sanvito, Z. Li, D. Wang, Y. Jiao, T. Liao, Q. Sun, Y. H. Ng, Z. Zhu, R. Amal and S. C. Smith, *Journal of the American Chemical Society*, 2012, **134**, 4393-4397.
7. C. Sun and D. J. Searles, *The Journal of Physical Chemistry C*, 2012, **116**, 26222-26226.
8. X. Luo, L.-M. Liu, Z. Hu, W.-H. Wang, W.-X. Song, F. Li, S.-J. Zhao, H. Liu, H.-T. Wang and Y. Tian, *The Journal of Physical Chemistry Letters*, 2012, **3**, 3373-3378.
9. Q. Yuan, J. Gao, H. Shu, J. Zhao, X. Chen and F. Ding, *Journal of the American Chemical Society*, 2012, **134**, 2970-2975.
10. C. Jin, F. Lin, K. Suenaga and S. Iijima, *Physical Review Letters*, 2009, **102**, 195505.
11. M. Chhowalla, H. S. Shin, G. Eda, L.-J. Li, K. P. Loh and H. Zhang, *Nat Chem*, 2013, **5**, 263-275.
12. RadisavljevicB, RadenovicA, BrivioJ, GiacomettiV and KisA, *Nat Nano*, 2011, **6**, 147-150.
13. W. S. Yun, S. W. Han, S. C. Hong, I. G. Kim and J. D. Lee, *Physical Review B*, 2012, **85**, 033305.
14. S. Fathipour, N. Ma, W. S. Hwang, V. Protasenko, S. Vishwanath, H. G. Xing, H. Xu, D. Jena, J. Appenzeller and A. Seabaugh, *Applied Physics Letters*, 2014, **105**, -.
15. T. Low, R. Roldán, H. Wang, F. Xia, P. Avouris, L. M. Moreno and F. Guinea, *Physical Review Letters*, 2014, **113**, 106802.
16. Y. Cai, G. Zhang and Y.-W. Zhang, *Sci. Rep.*, 2014, **4**.
17. H. Liu, A. T. Neal, Z. Zhu, Z. Luo, X. Xu, D. Tománek and P. D. Ye, *ACS Nano*, 2014, **8**, 4033-4041.
18. J. Qiao, X. Kong, Z.-X. Hu, F. Yang and W. Ji, *Nat Commun*, 2014, **5**.
19. Q. Yao, C. Huang, Y. Yuan, Y. Liu, S. Liu, K. Deng and E. Kan, *The Journal of Physical Chemistry C*, 2015, **119**, 6923-6928.
20. M.-L. Tsai, S.-H. Su, J.-K. Chang, D.-S. Tsai, C.-H. Chen, C.-I. Wu, L.-J. Li, L.-J. Chen and J.-H. He, *ACS Nano*, 2014, **8**, 8317-8322.
21. M. Buscema, D. J. Groenendijk, G. A. Steele, H. S. J. van der Zant and A. Castellanos-Gomez, *Nat Commun*, 2014, **5**.
22. A. N. Gandi and U. Schwingenschlögl, *Chemistry of Materials*, 2014, **26**, 6628-6637.
23. R. Fei, A. Faghaninia, R. Soklaski, J.-A. Yan, C. Lo and L. Yang, *Nano Letters*, 2014, **14**, 6393-6399.
24. Y. Shi, Y. Wang, J. I. Wong, A. Y. S. Tan, C.-L. Hsu, L.-J. Li, Y.-C. Lu and H. Y. Yang, *Sci. Rep.*, 2013, **3**.
25. F. Xia, D. B. Farmer, Y.-m. Lin and P. Avouris, *Nano Letters*, 2010, **10**, 715-718.
26. E. H. Hwang and S. Das Sarma, *Physical Review B*, 2008, **77**, 115449.
27. Y. Wang, M. Miao, J. Lv, L. Zhu, K. Yin, H. Liu and Y. Ma, *The Journal of Chemical Physics*, 2012, **137**, 224108.
28. R. S. Allgaier and W. W. Scanlon, *Physical Review*, 1958, **111**, 1029-1037.
29. I.-I. a. I.-I. C. Semiconductors: Group IV Elements, Landolt-Börnstein, New Series, Group III, Vol. 41, Pt. A, edited by O. Madelung, U. Rössler, and M. Schulz (Springer-Verlag, Berlin,

2005) .

30. S. J. Oh, N. E. Berry, J.-H. Choi, E. A. Gaulding, T. Paik, S.-H. Hong, C. B. Murray and C. R. Kagan, *ACS Nano*, 2013, **7**, 2413-2421.
31. K. Biswas, J. He, I. D. Blum, C.-I. Wu, T. P. Hogan, D. N. Seidman, V. P. Dravid and M. G. Kanatzidis, *Nature*, 2012, **489**, 414-418.
32. J. P. Heremans, V. Jovovic, E. S. Toberer, A. Saramat, K. Kurosaki, A. Charoenphakdee, S. Yamanaka and G. J. Snyder, *Science*, 2008, **321**, 554-557.
33. S. N. Girard, J. He, X. Zhou, D. Shoemaker, C. M. Jaworski, C. Uher, V. P. Dravid, J. P. Heremans and M. G. Kanatzidis, *Journal of the American Chemical Society*, 2011, **133**, 16588-16597.
34. M. Aerts, T. Bielewicz, C. Klinke, F. C. Grozema, A. J. Houtepen, J. M. Schins and L. D. A. Siebbeles, *Nat Commun*, 2014, **5**.
35. S. Goedecker, M. Teter and J. Hutter, *Physical Review B*, 1996, **54**, 1703-1710.
36. J. P. Perdew, K. Burke and M. Ernzerhof, *Physical Review Letters*, 1996, **77**, 3865-3868.
37. S. Grimme, *Journal of Computational Chemistry*, 2006, **27**, 1787-1799.
38. H. J. Monkhorst and J. D. Pack, *Physical Review B*, 1976, **13**, 5188-5192.
39. S. Takagi, A. Toriumi, M. Iwase and H. Tango, *Electron Devices, IEEE Transactions on*, 1994, **41**, 2357-2362.
40. S. Bruzzone and G. Fiori, *Applied Physics Letters*, 2011, **99**, -.
41. M. Gajdoš, K. Hummer, G. Kresse, J. Furthmüller and F. Bechstedt, *Physical Review B*, 2006, **73**, 045112.
42. A. Togo, F. Oba and I. Tanaka, *Physical Review B*, 2008, **78**, 134106.
43. K. Hummer, A. Grüneis and G. Kresse, *Physical Review B*, 2007, **75**, 195211.
44. A. K. Walton, T. S. Moss and B. Ellis, *Proceedings of the Physical Society*, 1962, **79**, 1065.
45. K. Kaasbjerg, K. S. Thygesen and K. W. Jacobsen, *Physical Review B*, 2012, **85**, 115317.
46. J. Xi, M. Long, L. Tang, D. Wang and Z. Shuai, *Nanoscale*, 2012, **4**, 4348-4369.
47. H. Peelaers and C. G. Van de Walle, *Physical Review B*, 2012, **86**, 241401.
48. C. E. Ekuma, D. J. Singh, J. Moreno and M. Jarrell, *Physical Review B*, 2012, **85**, 085205.